1   **Secondary Organic Aerosols from OH Oxidation of Cyclic Volatile Methyl Siloxanes as an Important**

2   **Si Source in the Atmosphere**

3   Chong Han[1], Hongxing Yang[1], Kun Li[2,3], Patrick Lee[2], John Liggio[2], Amy Leithead[2], Shao-Meng Li[4]*

4   [1]School of Metallurgy, Northeastern University, Shenyang, 110819, China

5   [2]Air Quality Research Division, Environment and Climate Change Canada, Toronto, Ontario M3H 5T4,

6   Canada

7   [3]Laboratory of Atmospheric Chemistry, Paul Scherrer Institute, Villigen 5232, Switzerland

8   [4]State Key Joint Laboratory of Environmental Simulation and Pollution Control, College of Environmental

9   Sciences and Engineering, Peking University, Beijing, China 100871

10   **Correspondence**: Shao-Meng Li (shaomeng.li@pku.edu.cn)

11

12   **Short summary:** We presented yields and compositions of Si-containing SOA generated from the reaction

13   of cVMS (D3-D6) with OH radicals. NO_x played negative roles on cVMS SOA formation, while ammonium

14   sulfate seeds enhanced D3-D5 SOA yields at short photochemical ages under high-NO_x conditions. The

15   aerosol mass spectra confirmed that the components of cVMS SOA significantly relied on OH exposure. A

16   global cVMS-derived SOA source strength was estimated to understand SOA formation potentials of cVMS.

17

18   **Abstract**

19   Cyclic volatile methyl siloxanes (cVMS) are active ingredients in widely used consumer products, which

20   can volatilize into the atmosphere, thus attracting much attention due to their potential environmental risks.

21   While in the atmosphere the cVMS undergo oxidation yielding both gaseous and particulate products. The

22   aerosol yields and compositions from the OH oxidation of four cVMS (D3-D6) were determined under low

23 and high-NO$_x$ conditions in an oxidation flow reactor. The aerosol yields progressively increased from D3

24 to D6, consistent with the volatilities and molecule weights of these cVMS. NO$_x$ can restrict the formation

25 of SOA, leading to lower SOA yields under high-NO$_x$ conditions than under low-NO$_x$ conditions, with a

26 yield decrease between 0.05-0.30 depending on the cVMS. Ammonium sulfate seeds exhibited minor

27 impacts on SOA yields under low-NO$_x$ conditions, but significantly increased the SOA yields in the oxidation

28 of D3-D5 at short photochemical ages under high-NO$_x$ conditions. The mass spectra of the SOA showed a

29 dependence of its chemical compositions on OH exposure. At high exposures, equivalent to photochemical

30 ages of > 4 days in the atmosphere, D4-D6 SOA mainly consisted of C_xH_y and $C_xH_yO_zSi_n$ under low-NO$_x$

31 conditions, whereas they primarily contained N_mO_z, C_xH_y, $C_xH_yO_1$, $C_xH_yO_{>1}$ and $C_xH_yO_zSi_n$ under high-NO$_x$

32 conditions. The potential contributions of cVMS to SOA formation in the atmosphere were evaluated using

33 the reported cVMS annual production and the yield data obtained in the present study. A global cVMS-

34 derived (D4-D6) SOA source strength is estimated to be 0.01 Tg yr^{-1}, distributed over major urban centers.

35

36 **1 Introduction**

37   Secondary organic aerosols (SOA), which contribute 50-85% to the mass of atmospheric organic aerosols

38 (OA) (Glasius and Goldstein, 2016), are mainly formed via the partitioning of low volatility products from

39 oxidation of volatile organic compounds (VOCs), semi- and intermediate volatile organic

40 compounds(S/IVOCs) (Riipinen et al., 2012). SOA has attracted significant attention due to their important

41 impacts on climate, ecosystems and human health (Berndt et al., 2016). Global budgets of SOA remain an

42 unresolved issue despite extensive research, largely due to uncertainties associated with aerosol yields and

43 the presence of unconsidered SOA precursors.

44   As one type of anthropogenic VOC and potential SOA precursors, cyclic volatile methyl siloxanes (cVMS)

45   are widely used in industrial applications and personal care products (Genualdi et al., 2011; Krogseth et al.,

46   2013a). cVMS have been classified as high-volume chemicals with an annual production of millions of tons

47   globally (Rücker and Kümmerer, 2015; Ahrens et al., 2014). Studies of cVMS in the environment have

48   focused on investigating health and environmental impacts particularly due to their potential persistence,

49   bioaccumulation and toxicity (Guo et al., 2019; Liu et al., 2018; Farasani and Darbre, 2017; Xu et al., 2019;

50   Kim et al., 2018; Coggon et al., 2018). As a result, the European Council has proposed a restriction on the

51   octamethylcyclotetrasiloxane (D4) and decamethylcyclopentasiloxane (D5) content in wash-off personal

52   care products to a limit of 0.1 mass% by 2020 (Eur-Lex, 2018). The legislative actions notwithstanding,

53   knowledge of environmental behavior of cVMS still needs to be further deepened as compared to their

54   applications and economic significance (Rücker and Kümmerer, 2015).

55   It has been estimated that approximately 90% of cVMS are emitted into the atmosphere due to their high

56   saturation vapor pressures (Allen et al., 1997). Gas-phase cVMS have been observed in both indoor and

57   outdoor air. Tang et al. (2015) reported that cVMS accounted for about one-third of total VOC mass

58   concentration in a classroom. Outdoor air concentrations of cVMS have also been measured at different sites

59   worldwide (Li et al., 2020; Wang et al., 2018; Rauert et al., 2018), increasing from rural to urban sites and

60   consistent with increasing population density (Rücker and Kümmerer, 2015). For example, at a rural site in

61   Sweden, the concentration of hexamethylcyclotrisiloxane (D3), D4, D5 and dodecamethylcyclohexasiloxane

62   (D6) were 0.94, 3.5, 13 and 1 ng/m^3, respectively (Kierkegaard and Mclachlan, 2013), while they were 18,

63   55, 172 and 14 ng/m^3 in urban areas of Toronto in Canada, respectively (Genualdi et al., 2011; Rauert et al.,

64   2018). cVMS have also been detected in the remote Arctic atmosphere, confirming their long-range transport

65   (Genualdi et al., 2011; Krogseth et al., 2013b). Atmospheric half-lives of cVMS are on the order of 30, 15,

66   10 and 6 days for D3-D6, respectively, which allow cVMS to exhibit a hemispherical distribution in the

67   atmosphere (Canada, 2008; Xiao et al., 2015). These lifetimes are driven mostly by reactions with the OH

68   radicals (Xiao et al., 2015; Wang et al., 2013), which generate silanols and dimeric products that can be

69   partitioned to condensed phases (Coggon et al., 2018; Sommerlade, 1993; Wu and Johnston, 2016). Different

70   OH concentrations can partly explain the seasonal variation of cVMS lifetimes that was characterized by

71   longer during winter than in summer (Rücker and Kümmerer, 2015). The loss of cVMS in the atmosphere is

72   negligible through O_3 and NO_3 due to their small reaction rates (Atkinson, 1991). The global loss by the

73   reaction with Cl atoms is less than 5% on account of low Cl concentrations, although it may be higher in

74   some regions where cVMS emissions and Cl sources overlap in both space and time (Alton and Browne,

75   2020). It has been demonstrated that elemental Si is a frequent constituent of nanoparticles in rural and urban

76   areas (Phares et al., 2003; Rhoads, 2003; Bein, 2005; Bzdek et al., 2014) and in remote regions (Li and

77   Winchester, 1990; Li and Winchester, 1993). These Si-containing nanoparticles have previously been

78   attributed to ore smelting processes, but recent studies have shown that Si-containing species are one of the

79   main components in cVMS SOA, suggesting that the oxidation of cVMS may be an important source of Si

80   in atmospheric aerosols (Wu and Johnston, 2016, 2017). In a modeling study, the oxidation products of

81   cVMS (D4, D5 and D6) were considered to quantify the maximum potential for aerosol formation through

82   reactions with the OH radicals (Janechek et al., 2017). Chandramouli and Kamens (2001) demonstrated the

83   gas-particle partitioning of silanols from D5 oxidation by the OH radicals. Wu and Johnston (2016, 2017)

84   analyzed the chemical composition of secondary aerosols from OH oxidation of D4 and D5, showing a large

85   number of monomeric and dimeric products. Janechek et al. (2017, 2019) reported physical properties of

86   SOA generated by OH oxidation of D5, including hygroscopicity, cloud seeding potential and volatility.

87   Charan et al. (2022) measured SOA yields of D5 using chambers and flow tube reactors, emphasizing the

88   importance of the relevant OH concentrations and exposures when extrapolating these laboratory results or

89 comparing with other studies. These studies mainly focused on D5 and occasionally D4 but rarely others. To

90 better understand the SOA-forming potentials of typical cVMS in the atmosphere, accurate yields and

91 molecular compositions of SOA from the oxidation of cVMS under various atmospheric conditions are

92 needed.

93   In this work, the formation of SOA from the oxidation of four cVMS (D3-D6) by OH radicals was

94 investigated in an oxidation flow reactor (OFR). Under various combinations of NO_x and ammonium sulfate

95 seed concentrations, the yields and compositions of SOA formed from the oxidation were measured using a

96 suite of instruments including a scanning mobility particle sizer (SMPS), a proton transfer reaction time of

97 flight mass spectrometer (PTR-ToF-MS) and an aerosol mass spectrometer (AMS). Based on these SOA

98 yields, the contribution of cVMS to SOA in the global atmosphere was estimated using reported cVMS

99 concentrations. The results obtained here can largely improve our understanding of the contribution and

100 composition of SOA from cVMS.

101 **2 Experiments and methods**

102 **2.1 Photo-oxidation experiments**

103   The reactions of cVMS with OH radicals were controlled at a constant temperature ($21\pm1^\circ$C) and relative

104 humidity ($35\%\pm2\%$) in a custom-made oxidation flow reactor (the Environment and Climate Change Canada

105 oxidation flow reactor, ECCC-OFR), which is shown in Fig. S1 of the Supplement and has been described

106 in detail previously (Li et al., 2019a). Briefly, the ECCC-OFR is a fused quartz cylinder (length: 50.8 cm,

107 inner diameter: 20.3 cm) equipped with a conical inlet and 7 outlets. Wall losses of particles and gases in the

108 ECCC-OFR have been shown to be lower than in other OFRs (Huang et al., 2017; Lambe et al., 2011;

109 Simonen et al., 2017; Li et al., 2019a). The length and full angle of cone inlet are 35.6 cm and 30°,

110 respectively, designed to minimize the formation of jetting and recirculation in the OFR. The outlet at the

111   reactor center is a stainless-steel sampling port (inner diameter: 0.18 in) extending 12.7 cm long into the

112   ECCC-OFR. This sampling inlet reduces the impact of potential turbulent eddies caused by the back end of

113   the reactor. The remaining 6 outlets around the perimeter are designed to allow side flows to pass through

114   the OFR as a sheath flow, indirectly reducing wall losses of gases and particles inside the OFR upon sampling.

115   Ozone-free mercury UV lamps for generating OH radicals are housed in small quartz tubes around and in

116   parallel to the quartz reaction cylinder, and a large flow of air through each of these smaller quartz tubes is

117   used to remove the heat produced by the lamps. The relative humidity was adjusted by controlling the ratio

118   of dry air to wet air into the reactor, and was measured using a humidity sensor (Vaisala) at one of the sheath

119   flow outlets (side flows) of the reactor. The volume of the entire ECCC-OFR is about 16 L and the total flow

120   rate is 8 L min^{-1}, leading to a residence time of 2 min in the OFR.

121   OH radicals were produced through the reaction of water vapor with O(^{1}D) formed from O$_3$ photolysis at

122   254 nm. The OH concentration in the ECCC-OFR was regulated by controlling the input voltage and the

123   number of UV lamps. Methanol vapor, introduced into the ECCC-OFR through a bubbler containing

124   methanol solution, was used to determine the OH exposure (i.e., photochemical age, from the multiplication

125   of OH concentration and reaction time) by tracking its decay in the reactor from the reaction with the OH.

126   The decay, or fractional loss, of gas-phase methanol, $[MeOH]/[MeOH]_0$ was measured with the PTR-ToF-

127   MS, and was used to calculate the OH concentration via Equation 1,

$$[OH]=-\frac{1}{k_{MeOH}}\ln\frac{[MeOH]}{[MeOH]_0} \tag{1}$$

129   where k_{MeOH} is the second-order rate constant of methanol reaction with OH at 298 K (9.4×10^{-13} cm^3

130   molecule^{-1} s^{-1}). The OH exposure measurement was offline, because methanol can affect the OH reactivity

131   with cVMS. Under low and high-NO$_x$ conditions described below, the OH exposure varied in the range of

132   5.5×10^{10}-1.8×10^{12} and 8.2×10^{10}-1.1×10^{12} molecules cm^{-3} s, respectively. They correspond to 0.4-14.2

133   and 0.6-8.5 equivalent days (photochemical age), respectively, assuming that an average OH concentration

134   in air is 1.5×10^6 molecules cm^{-3} (Mao et al., 2009).

135   Pure D3-D6 cVMS compounds (solid D3 and liquid D4, D5 and D6) were placed in a glass U-type tube

136   and maintained at room temperature. Vapors from these compounds (Table S1 of the Supplement) were

137   separately introduced into the ECCC-OFR by a small flow of zero air (1-18 mL min^{-1}) passing over the

138   headspace of the U-tube containing the pure compounds. The concentrations of D3-D6 in the ECCC-OFR

139   ranged from 20 to 43 ppb (Table S2), depending on their volatilities. Table S2 summarizes the concentrations

140   of cVMS at the reactor inlet and outlet, when the OH exposure was 1.85×10^{12} and 1.10×10^{12} molecules cm^{-3} s in low and high-NO_x experiments, respectively, indicating the reaction depth of cVMS. To study the

142   influence of existing particles on the SOA formation, ammonium sulfate (AS) seed particles were produced

143   using an atomizer, dried by a diffusion dryer and neutralized by a neutralizer and injected into the reactor

144   without size selection. The mass concentration of AS seed particles was approximately 30 µg m^{-3} for all

145   experiments.

146   N_2O was used as a source of NO to achieve high-NO_x conditions (Lambe et al., 2017). NO_x conditions

147   were defined by the fate of peroxy radicals (RO_2), which was described by the reaction rate ratio (R_{NO}) of

148   RO_2 + NO and RO_2 + HO_2 (Peng et al., 2018). The R_{NO} ratio increases with increasing OH exposures at a

149   constant concentration of N_2O (Li et al., 2019b). To achieve a constant branching ratio during the high-NO_x

150   experiments, the initial N_2O concentration in the OFR was varied (1.6%-8.0%) to maintain an R_{NO} value of

151   20 (Li et al., 2019b), as calculated using a model (OFR Exposures Estimator v3.1) (Peng et al., 2018). A

152   ratio of R_{NO}=20 indicates that 95% of RO_2 reacts with NO, ensuring the dominance of RO_2 + NO, which

153   represents conditions that are relevant for urban atmosphere (Peng et al., 2019). The role of RO_2 + RO_2 here

154   should be minor or negligible due to the low concentration of SOA precursors (cVMS, 18-46 ppb) (Lambe

155   et al., 2017; Peng et al., 2019; Li et al., 2019b). Peng et al. (2019) have reported that in the experiments

156   utilizing the injection of N_2O to achieve high-NO_x conditions, the relative importance of RO_2 + OH was

157   generally negatively correlated with N_2O due to the suppressing effect of NO_x on OH radicals and the

158   increasing role of RO_2 + NO. Under low-NO_x conditions, N_2O was not introduced into the OFR, where the

159   reaction ratio of RO_2 with HO_2 was estimated to be larger than 99% according to the model mentioned above

160   (Peng et al., 2018), representing atmospheric scenarios with few NO_x sources.

161   **2.2 Characterization and analysis**

162   The concentrations of cVMS in the OFR were measured online with PTR-ToF-MS (Ionicon Analytik

163   GmbH) (Liggio et al., 2016). The number and mass size distribution of aerosols was monitored using a

164   scanning mobility particle sizer (SMPS, TSI). The mass spectra and elemental composition of aerosols was

165   determined with a high-resolution time-of-flight aerosol mass spectrometer (HR-ToF-AMS, Aerodyne) and

166   analyzed with the AMS analysis software Squirrel (version 1.62G) and Pika (version 1.22G).

167   SOA mass yields (Y) were calculated via Equation 2,

168    $$Y = \frac{\Delta C_{SOA}}{\Delta C_{cVMS}} \tag{2}$$

169   where ΔC_{SOA} and ΔC_{cVMS} are the mass concentrations of SOA formed and cVMS lost, respectively. The mass

170   concentration of SOA was determined by multiplying the effective aerosol density by the integrated SOA

171   volume concentration from the SMPS, subtracting the AS seed volume for experiments with AS seeds. The

172   effective aerosol density (ρ) was calculated for unseeded experiments through the following Equation 3

173   (Lambe et al., 2015),

174    $$\rho = \frac{D_{va}}{D_m} \tag{3}$$

175   where D_{va} is the vacuum aerodynamic diameter obtained from the HR-ToF-AMS, and D_m is the electric

176   mobility diameter measured by the SMPS. The ρ varied in the range of 1.6-1.8 depending on the cVMS. The

177 same ρ value was also used in the seeded experiments. It should be pointed out that the background values

178 in Table S3 have been subtracted when calculating the cVMS SOA yields. The average data of SMPS and

179 AMS in the last ~10 minutes for each OH exposure was used to calculate the SOA yields (inset of Fig S2),

180 which can reduce the deviation caused by unstable SOA loadings at high OH exposures.

3 Results and discussion

3.1 SOA yields

183 Taking the D5 SOA under unseeded conditions as an example, the number and mass size distributions of

184 aerosols were shown in Fig. S3 at three photochemical ages (PA), i.e., time-integrated OH exposure. It can

185 be seen that small particles dominated the total particle number counts, while large ones dominated the mass.

186 The mass mode diameter of SOA for mass size distributions increased with PA under low and high-NO_x

187 conditions. The mass concentrations and time series of SOA obtained from SMPS and AMS were shown in

188 Table S4 and Fig. S2, respectively, which reflected a step-by-step pattern with increasing OH exposures.

189 Unstable SOA loadings at high OH exposures may be attributed to the fragmentation reactions, leading to

190 the difficulty in the deposition of products on SOA.

191 Figure 1 shows the SOA yields from the photooxidation of the D3-D6 cVMS under low and high-NO_x

192 conditions as a function of PA, with and without AS seed particles. SOA yields have been widely used to

193 estimate the potential of precursors to produce aerosol mass (Mcfiggans et al., 2019; Li et al., 2019a; Bruns

194 et al., 2015; Lambe et al., 2015). As shown in Fig. 1, the cVMS SOA yields exhibited an overall increasing

195 trend with PA, expressed in equivalent photochemical days, which agreed with the trend of D5 SOA yields

196 reported by Janechek et al. (2019). Under low-NO_x conditions (Fig. 1a), SOA yields exhibited a slow growth,

197 reaching a plateau after 10 equivalent days. This may be due to increased gas-phase fragmentation of cVMS

198 to generate some higher volatility products, leading to a small increasing amplitude of partition ratio of

199   species into SOA at longer photochemical ages.
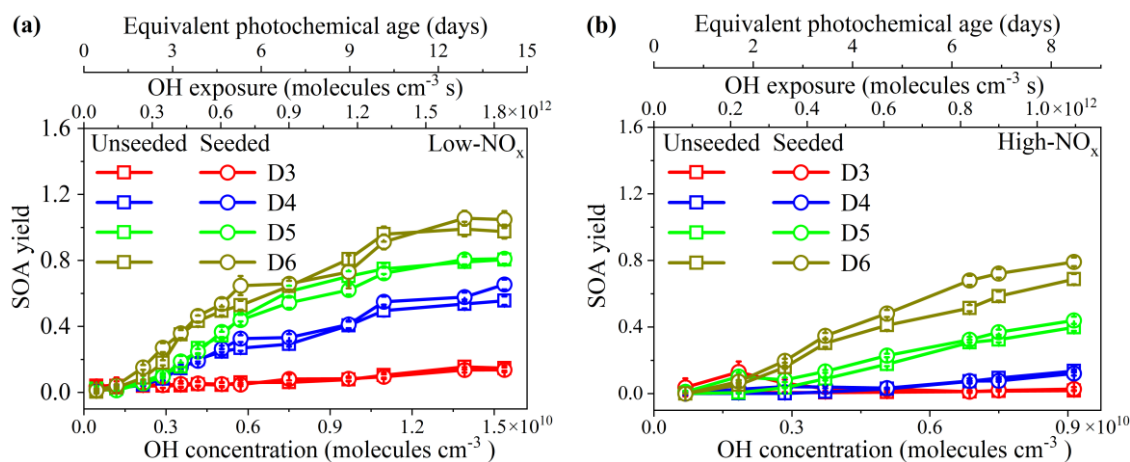
201   Figure 1. SOA yields from unseeded and seeded (30 µg m^{-3}) photooxidation of cVMS by OH radicals. (a)

202   low-NO$_x$ experiments; (b) high-NO$_x$ experiments.

203

204   For the unseeded and low-NO$_x$ experiments in Fig. 1a, SOA yields of four cVMS exhibited significant

205   differences in values over the same number of equivalent days. The SOA yields successively increased from

206   D3 to D6, consistent with the volatilities and molecular masses of the cVMS as well as their reaction rate

207   constants with the OH radical (Alton and Browne, 2020; Kim and Xu, 2017; Safron et al., 2015). The

208   maximum SOA yields of D3-D6 were (0.16±0.02), (0.56±0.03), (0.80±0.03) and (0.99±0.04), respectively,

209   occurring after a PA of 12 equivalent days. It has been reported that D5 SOA yields varied in the range of 0-

210   1.1 (Janechek et al., 2019; Wu and Johnston, 2017; Charan et al., 2022). Under a low OH exposure (~10^{10}-

211   10^{11} molecules cm^{-3} s), the D5 SOA yield (0.01-0.11) obtained here was similar to that (chamber, 0-0.057;

212   flow tube, 0.018-0.06) measured by Charan et al. (2022). However, under a high OH exposure of ~10^{11}-10^{12}

213   molecules cm^{-3} s, the D5 SOA yield of 0.46-0.70 was higher than 0.22 and 0.14-0.35 (flow tube) reported

214   by Janechek et al. (2019) and Charan et al. (2022), respectively, which may be attributed to differences in

215   experimental conditions, such as differences in reactors, wall losses, SOA measurement methods,

216   determination of OH concentrations, and initial D5 concentrations (Table S5) (Janechek et al., 2019; Charan

10

217   et al., 2022). Although the amount of cVMS lost was variable, cVMS SOA yields positively depended on

218   SOA mass concentrations (Fig. S4), and this trend was observed in previous D5 SOA experiments with OH

219   oxidation (Wu and Johnston, 2017).

220   As shown in Fig. 1b, the order of SOA yields from the four cVMS under high-NO_x conditions was the

221   same as that under low-NO_x conditions. However, the SOA yields under high-NO_x conditions were generally

222   smaller than the corresponding yields at similar OH exposures under low-NO_x conditions, with a decrease

223   of 0.05-0.30 depending on the cVMS. Such a reduction suggests that NO_x can restrict the formation of cVMS

224   SOA. NO_x has been shown to reduce SOA yields for some anthropogenic alkanes (Li et al., 2019b), aromatics

225   (Ng et al., 2007a; Chan et al., 2009; Zhou et al., 2019), monoterpenes (Zhao et al., 2018) and other terpenes

226   (Ng et al., 2007b), attributable to the formation of higher volatility products (e.g., organic nitrates) generated

227   by RO_2 + NO compared to RO_2 + HO_2 (Presto et al., 2005; Li et al., 2019b), which is also likely the case

228   here. The higher volatility products favor partitioning in the gas phase, thus reducing the potential for

229   forming SOA (Zhou et al., 2019). Moreover, high NO_x levels can suppress the formation of products for

230   nucleation, thereby reducing aerosol surface as a condensational sink and increasing the wall loss of

231   condensable species in an OFR under high-NO_x conditions (Zhao et al., 2018; Sarrafzadeh et al., 2016; Wildt

232   et al., 2014). Figure S5 indicates that the difference between SOA yields with and without NO_x decreased

233   with increasing silicon atoms within individual cVMS, indicating a less restricting effect of NO_x on the SOA

234   formation for larger cVMS. This means that high NO_x levels play a lessor role in the SOA yields of lower

235   volatility precursors.

236   SOA yields in the AS-seeded experiments under low and high-NO_x conditions are also shown in Figs. 1

237   and S5, indicating minimal impacts of the AS seed particles on SOA yields. A yield enhancement ratio

238   ($R_E = Y_{seeded}/Y_{unseeded}$, Fig. S6) was used to show the seed impacts more clearly. Under low-NO_x conditions,

239 the R_E values for all cVMS were close to 1.0 (Fig. S6a), suggesting a negligible impact of AS seed particles

240 on SOA yields; however, under high-NO$_x$ conditions, R_E was much larger (17.81, 13.18 and 15.51 for D3-

241 D5, respectively) at short PA but gradually decreased to 1.0 with increasing PA for D3-D5, while it was

242 always close to 1.0 for D6 regardless of PA (Fig. S6b). R_E values greater than 1.0 suggest that AS seed

243 particles played an enhancement role in the cVMS SOA formation, as similarly reported in SOA formation

244 from hydrocarbons (Sarrafzadeh et al., 2016; Lamkaddam et al., 2017; Li et al., 2019b). Under low-NO$_x$

245 conditions, the general lack of impact on cVMS SOA yields by the AS seed particles suggests that

246 condensation was not the main process driving SOA formation in cVMS oxidation. For the few cases of high

247 NO$_x$ level at low PA, where R$_E$ was >1 for D3-D5, it is possible that their early generations of oxidation

248 products were more volatile than successive generations of products and hence more prone to condensation

249 enhanced by AS seeds. As PA increased, further reactions of these early generation oxidation products with

250 OH radicals resulted in further generation products that were likely less volatile, thereby weakening the

251 enhancing role of AS seeds at high OH exposure. Such effect was less pronounced for D6, likely because its

252 oxidation products at different PA had similar volatilities. Figure S6b shows that the effect of AS seed

253 particles on SOA yields negatively correlated with the number of silicon atoms in the cVMS. Lower volatility

254 precursors (D5 and D6) may form lower volatile products, resulting in SOA yields less sensitive to the pre-

255 existing seeds.

256 **3.2 Aerosol compositions**

257 **3.2.1 Compositions of SOA under low-NO$_x$ conditions.**

258 Figures 2 and S7 show the normalized HR-ToF-AMS mass spectra of cVMS SOA from unseeded

259 experiments under low-NO$_x$ conditions at OH exposures of 9.0×10^{11} molecules cm^{-3} s (i.e., OH

260 concentration of 7.5×10^9 molecules cm^{-3}). The mass spectral signals can be identified as fragments with a

261 formula of $C_xH_yO_zSi_n$. For D3 SOA, the most prominent peaks were at m/z 44 and 29, dominated by CO_2^+

262 and CHO^+, which were tracers for organic acids (Ng et al., 2010), alcohols and aldehydes (Lee et al., 2012),

263 respectively. They may result from the oxidation of the methyl groups in D3 by OH radicals. For the mass

264 spectra of D4-D6 SOA, the two highest peaks at m/z 14 and 15 were CH_2^+ and CH_3^+, respectively. In addition,

265 there were several dominant $C_xH_yO_zSi_n$ peaks, which were fragments of silicon-containing products. For the

266 $C_xH_yO_zSi_n$ group in D4 SOA, there were four typical peaks at m/z 255, 257, 271 and 273, with formulae of

267 $C_4H_{11}O_7Si_3^+$, $C_3H_9O_8Si_3^+$, $C_3H_7O_9Si_3^+$ and $C_3H_9O_9Si_3^+$, respectively. The $C_xH_yO_zSi_n$ fragment group

268 containing Si of D5 SOA had three dominant peaks at m/z 327, 329 and 331, corresponding to $C_{12}H_{11}O_2Si_5^+$,

269 $C_9H_9O_8Si_3^+$ and $C_5H_{15}O_9Si_4^+$, respectively. For the $C_xH_yO_zSi_n$ group containing Si in D6 SOA, there were

270 five main peaks at m/z 73 (C_3H_9Si), 387 ($C_8H_{23}O_8Si_5^+$), 389 ($C_8H_9O_9Si_5^+$), 401 ($C_9H_{21}O_{10}Si_4^+$) and 403
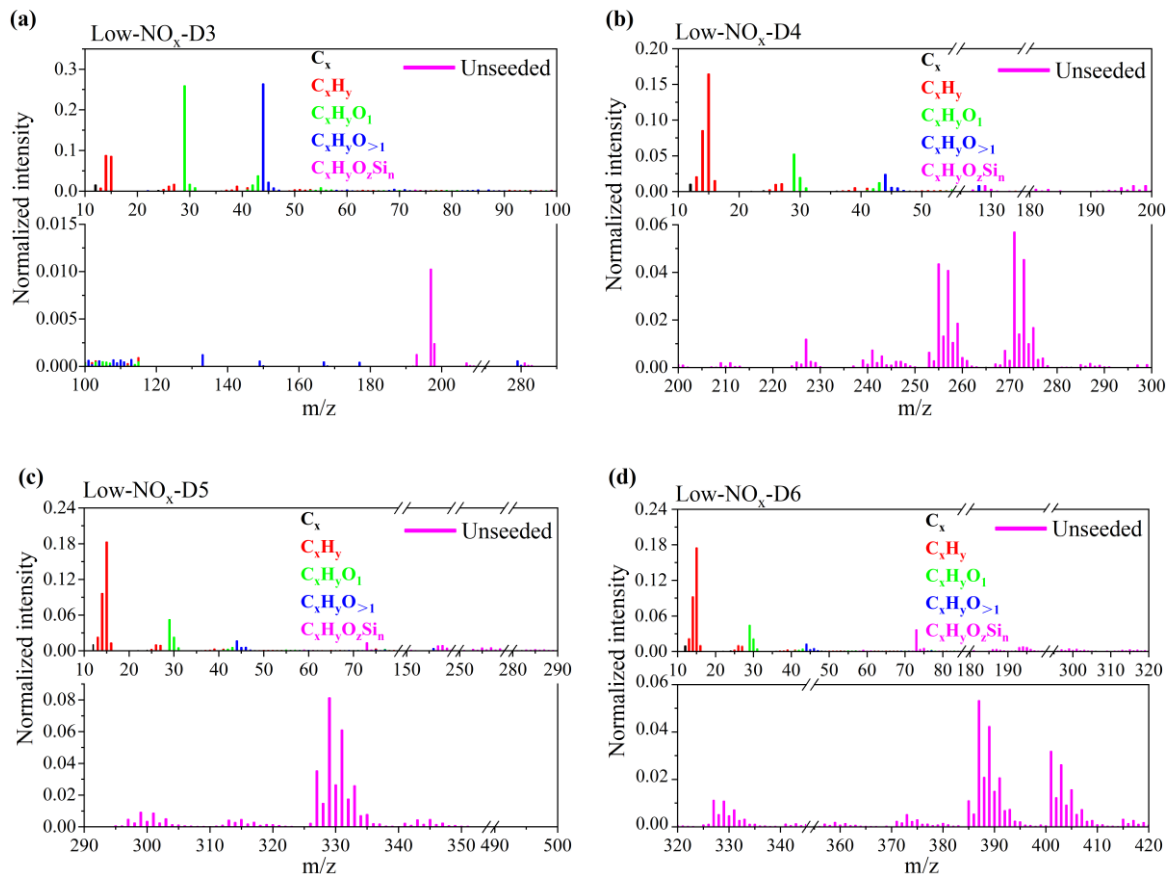
271 ($C_7H_{15}O_{12}Si_4^+$).

Figure 2. HR-ToF-AMS mass spectra of cVMS SOA at OH exposure of 9.0×10^{11} molecules cm^{-3} s (i.e.,

OH concentration of 7.5×10^{9} molecules cm^{-3}) under low-NO$_x$ conditions in unseeded experiments. a-d

represent the mass spectra of D3-D6 SOA, respectively.

Figure 3 shows the evolution of different groups of ions in the HR-ToF-AMS spectra of the cVMS SOA

as a function of PA in equivalent days. For D3-D6 under unseeded conditions, $C_xH_yO_1$ and $C_xH_yO_{>1}$ ions

significantly decreased within 0-4 equivalent days of PA, but remained essentially unchanged when PA

increased to 7-15 equivalent days. The C_xH_y ion increased to its peak value at about 9 equivalent days of PA

for D3 and 2-3 equivalent days of PA for D4-D6, and then gradually decreased with further PA increases.

The $C_xH_yO_zSi_n$ group of ions maintained an increasing trend until 9-10 days of PA, thereafter it decreased

slightly for D4-D6 SOA.

14

285   The weighted values of the Si/C (n/x) and Si/O (n/z) atomic ratios for the $C_xH_yO_zSi_n$ groups in D5 and D6

286   SOA at different PA are plotted in Fig. S8 (Detailed calculations in Text S1 of the Supplement), which can

287   be used to indicate the changes in the Si element of SOA. The Si/C ratio increased slightly with increasing

288   PA, whereas the Si/O ratio had an overall decrease trend. While it is difficult to separate the effect of

289   fragmentation due to the AMS ionization process, the relative changes of group intensities and the evolution

290   of Si/C and Si/O in $C_xH_yO_zSi_n$ over different PA may be attributed to the evolution of cVMS when oxidized

291   by the OH radicals. The initial step of OH radical oxidation is H abstraction from the methyl groups on the

292   -Si-O- ring of the cVMS to form Si-containing radicals, which may generate OH and CH_2OH substitution

293   products, such as silanol and silyl methanol (Wu and Johnston, 2016; Alton and Browne, 2020). Such Si-

294   containing products may partition into SOA and result in an appearance of $C_xH_yO_zSi_n$ ions in the AMS mass

295   spectra.   Notably,   it   was   reported   that   one   of   oxidation   products   of   D5,   1-

296   hydroxynonamethylcyclopentasiloxane (D_4TOH), has been detected in ambient particulate matter (Milani et

297   al., 2021). At low PA, some oxygen-containing functional groups (-CH_2OH/-COOH/-OH), which were

298   formed by the reaction of methyl groups in cVMS with OH, resulted in a decrease of Si/O ratio. The Si-O

299   bond breaking may mainly happen at high OH exposures, and it may occur after the cleavage of Si-C bonds

300   (Rücker and Kümmerer, 2015). According to the previous study of Wu and Johnston (2017), some ring-

301   opened products were generated from the reaction of D5 with OH radicals, necessarily requiring the cleavage

302   of Si-O bonds. The Si-O bond cleavage from the OH radical attack may reduce the number of Si atoms,

303   leading to a continuous decrease of Si/O at high PA. The continued breaking of Si-O bonds would lead to

304   fragmentation and more volatile products, which caused lower SOA yield and $C_xH_yO_zSi_n$ fraction at longer

305   PA (Figs. 1 and 3). The field measurements observed that Si acts as a frequent component of atmospheric

306   nanoparticles (Bzdek et al., 2014). This work further determines that cVMS SOA could become an important

15

307   contributor to Si in aerosols.
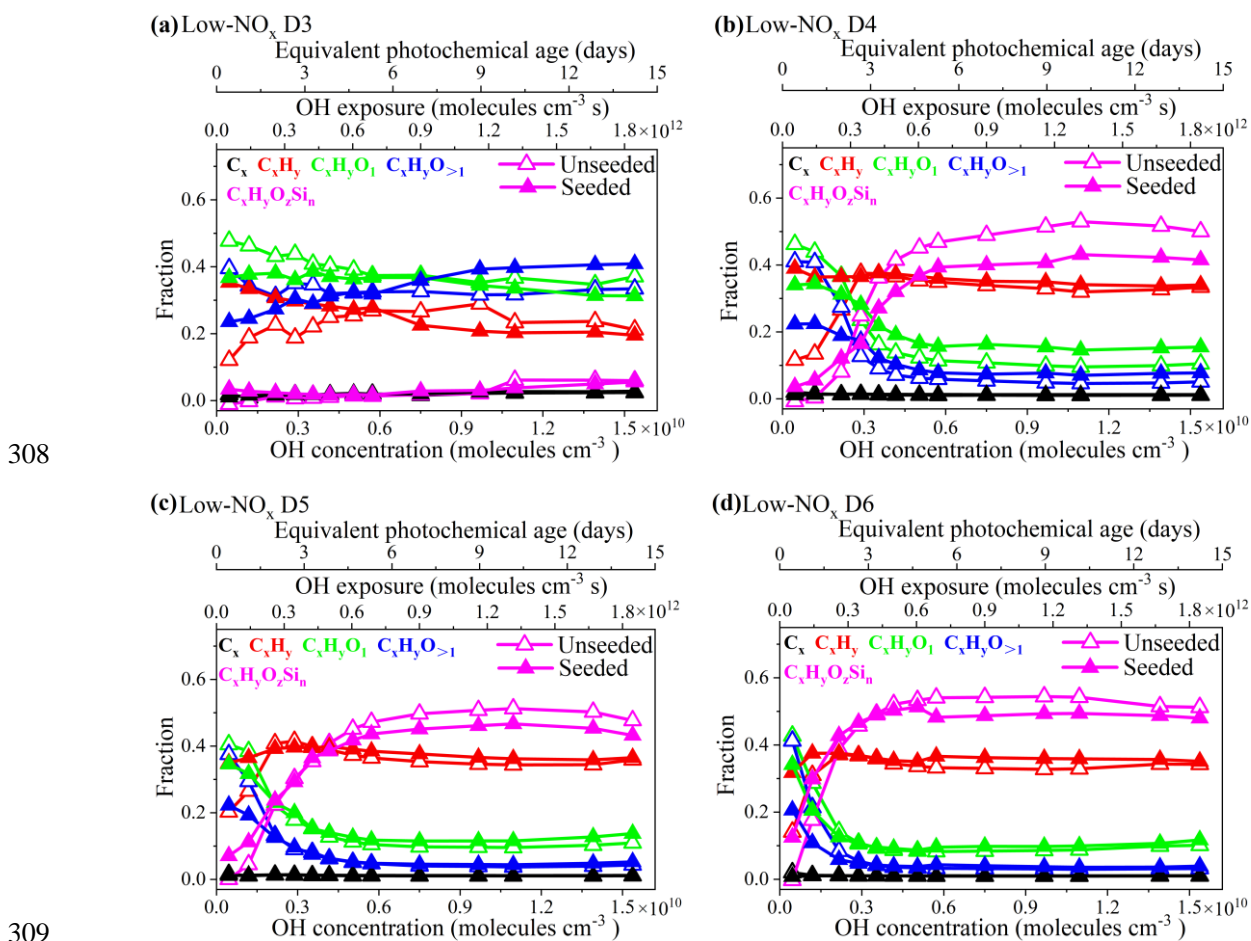
Figure 3. Fraction of C_x, C_xH_y, $C_xH_yO_1$, $C_xH_yO_{>1}$ and $C_xH_yO_zSi_n$ ion groups for SOA derived from the

oxidation of cVMS (a-d) by OH radicals at different photochemical ages under low-NO_x conditions.

Empty and solid triangles represent experimental data under unseeded and seeded conditions, respectively.

313

As shown in Fig. 3, the presence of seeds led to some changes in the evolution trends of ion groups in the

AMS spectra. For instance, the initial fraction of C_xH_y in seeded experiments was larger than that in unseeded

experiments, which may be related to the volatility of species containing C_xH_y that may be more easily

deposited in the presence of seeds, whereas $C_xH_yO_1$ and $C_xH_yO_{>1}$ exhibited opposite changes. The presence

of seeds led to larger initial and smaller steady-state $C_xH_yO_zSi_n$ fractions than those in unseeded experiments.

Regardless of the presence of seeds, C_xH_y, $C_xH_yO_1$ and $C_xH_yO_{>1}$ mainly contributed to the composition of

16

320   all cVMS SOA at initial OH radicals oxidation, but D4-D6 SOA primarily consisted of C_xH_y and $C_xH_yO_zSi_n$

321   after 4 equivalent days.

3.2.2 Compositions of SOA under high-NO$_x$ conditions.

323   Figure S9 shows the HR-ToF-AMS mass spectra of cVMS SOA from unseeded experiments under high-

324   NO$_x$ conditions at OH exposures of 9.0×10^{11} molecules cm^{-3} s (~6.9 d). Compared to that under low-NO$_x$

325   conditions (Figs. 2 and S7), there was one additional N-containing group (N_mO_z) in the SOA mass spectra

326   under high-NO$_x$ conditions, which accounted for 16%-31%. For the mass spectra of D3-D6 SOA originating

327   from unseeded experiments under high-NO$_x$ conditions in Fig. S9, the dominating peaks of the N_mO_z family

328   were m/z 30 (NO$^+$) and m/z 46 (NO$_2^+$). The common main peaks were located at m/z 30 (NO$^+$) for cVMS

329   SOA, m/z 44 (CO$_2^+$) for D3-D4 SOA, and m/z 46 (NO$_2^+$) for D4-D6 SOA. In addition, there were other

330   primary peaks at m/z 29 (CHO$^+$) for D4 SOA, while m/z 15 (CH$_3^+$) and m/z 28 (CO$^+$) for D5-D6 SOA. The

331   m/z 28 (CO$^+$), similar to m/z 44 (CO$_2^+$), is considered as a tracer for organic acids (Ng et al., 2010). In the

332   mass spectra for D3-D6 SOA under high-NO$_x$ conditions, the presence of NO$^+$ (m/z 30) and NO$_2^+$ (m/z 46)

333   illustrated the formation of organic or inorganic nitrates in SOA (Ng et al., 2007b; Zhao et al., 2018).

334   For the $C_xH_yO_zSi_n$ group in the D4 SOA mass spectrum under high-NO$_x$ conditions, the dominating peaks

335   and their formulas were the same as those under low-NO$_x$ conditions. For the $C_xH_yO_zSi_n$ group in D5 SOA,

336   in addition to two typical peaks at m/z 327 and 329 in the low-NO$_x$ experiments, there was another prominent

337   peak at m/z 328, with a formula $C_8H_{12}O_5Si_5$. The $C_xH_yO_zSi_n$ group in D6 SOA had three typical peaks at m/z

338   73 (C$_3$H$_9$Si), m/z 387 (C$_8$H$_{23}$O$_8$Si$_5^+$) and m/z 401 (C$_9$H$_{21}$O$_{10}$Si$_4^+$). For the $C_xH_yO_zSi_n$ groups in cVMS SOA,

339   there was little difference in the x, y, z and n value assignment of $C_xH_yO_zSi_n$ peaks in SOA generated under

340   low-NO$_x$ and high-NO$_x$ conditions, suggesting the formation of similar Si-containing oxidation products.

341   For cVMS SOA under high-NO$_x$ conditions, the evolution of family groups as a function of OH exposure

342   was summarized in Fig. S10. The dominant composition at the initial stage was $C_xH_yO_{>1}$ groups for D3-D6

343   SOA. At equivalent days larger than 4, D3 SOA primarily consisted of $C_xH_yO_{>1}$, N_mO_z and $C_xH_yO_1$ groups,

344   while D4-D6 SOA was mainly composed of $C_xH_yO_zSi_n$, N_mO_z, $C_xH_yO_1$, C_xH_y and $C_xH_yO_{>1}$ groups. Figure

345   S10 also shows influences of seeds on the evolution of family groups under high-NO_x conditions. It was

346   observed that all groups in D3-D6 SOA displayed similar change trends regardless of the existence of seeds.

347   As shown in Fig. S11, the trend of the Si/O ratio in the $C_xH_yO_zSi_n$ groups at different photochemical ages

348   under high-NO_x conditions was similar to that in low-NO_x experiments. However, the Si/C ratios remained

349   almost unchanged, and were close to the initial value (0.5) in cVMS. This may be attributed to the possible

350   suppression of cleavage of methyl groups from the -Si-O- ring of the cVMS under high-NO_x conditions.

4 Conclusions and implications

352   The yields and compositions of SOA generated from the photooxidation of four cVMS (D3-D6) with OH

353   radicals were investigated using an oxidation flow reactor. cVMS SOA yields exhibited an overall increasing

354   trend with PA, and their values gradually increased with cVMS from D3 to D6. SOA formations depended

355   on NO_x, as shown by smaller SOA yields under high-NO_x conditions. Ammonium sulfate seeds significantly

356   enhanced SOA yields of D3-D5 at short PA under high-NO_x conditions. The SOA mass spectra showed that

357   Si-containing species were one of main chemical compositions at PA > 4 days.

358   To evaluate the potential contributions of cVMS to SOA formation in the atmosphere, global SOA

359   concentrations produced from cVMS were estimated according to the cVMS SOA yields measured in this

360   work and using the cVMS concentrations reported from multiple studies, which were listed in Table S6.

361   Figure 4 shows the global concentration distribution of SOA from four cVMS (D3-D6) at 36 sites worldwide

362   estimated by the Equation 4,

363
$$C_{cVMS\text{-}SOA} = C_{cVMS} \times \frac{\Delta C_{cVMS}}{C_{in\text{-}cVMS}} \times Y \tag{4}$$

364   where C_{cVMS} and $C_{cVMS-SOA}$ are the mass concentration of cVMS reported from literatures and cVMS SOA

365   estimated in global sites, respectively; $C_{in-cVMS}$ and ΔC_{cVMS} are the mass concentration of initial and lost

366   cVMS at the selected equivalent days during the experiments of this work, respectively (Table S7); Y is the

367   cVMS SOA mass yields selected here. The estimations from the Equation 4 were based on assumptions that

368   the lost cVMS ratio is not affected by the cVMS concentration and the background $C_{cVMS-SOA}$ is zero. The

369   dilution of cVMS would occur during the transportation in the atmosphere, leading to an uncertainty of

370   cVMS concentrations (C_{cVMS}) in the Equation 4. To simplify the estimation process, the effect of dilution on

371   C_{cVMS} would not be taken into account, and the reported C_{cVMS} values were directly used. It was noted that

372   the time-integrated consumption over the lifetime of a precursor compound in the atmosphere should be

373   suitable for evaluating the SOA formation. Accordingly, when considering atmospheric half-lives (6-30 days)

374   of cVMS, the $\Delta C_{cVMS}/C_{in-cVMS}$ values in low-NO$_x$ and unseeded experiments at 14.2 equivalent days (Table

375   S7) are used to calculate cVMS SOA at background and polar sites. Due to a short residence time of airmass

376   over urban areas, the $\Delta C_{cVMS}/C_{in-cVMS}$ values in high-NO$_x$ and seeded experiments at 0.63 equivalent days

377   (Table S7) are employed to estimate cVMS SOA at urban sites.

378   It should be noted that OH concentrations and exposures have different effects on the reaction systems,

379   leading to different SOA yields. Under an ideal condition, a low OH concentration for a long exposure time

380   and a high OH concentration for a short exposure time can achieve the same degree of degradation of the

381   precursor compound. However, this is not applicable for the formation of SOA. Charan et al. (2022) have

382   claimed that D5 SOA yields are dependent on the OH concentrations rather than OH exposures. When

383   extrapolating the laboratory data to the real atmosphere, it is necessary to consider atmospherically relevant

384   OH concentrations and exposures. Charan et al. (2022) also stated that the D5 SOA yield varied in a small

385   range (0-6%) at the OH concentration $\leq 5 \times 10^8$ molecules cm^{-3}. It was assumed that the SOA yields at

386   environmentally relevant OH concentrations ($\sim10^6$ molecules cm^{-3}) were similar to those at the lowest OH

387   concentrations ($\sim10^8$ molecules cm^{-3}) used here. Thus, the high-NO$_x$ SOA yields (D3: 0.038; D4: 0.001; D5:

388   0.011; D6: 0.000) under the seeded conditions at the OH concentration of 6.83×10^8 molecules cm^{-3} (0.63

389   equivalent days) were employed in the calculation of cVMS SOA concentrations at urban sites, while the

390   low-NO$_x$ SOA yields (D3: 0.041; D4: 0.013; D5: 0.023; D6: 0.004) under the unseeded conditions at the OH

391   concentration of 4.57×10^8 molecules cm^{-3} (0.42 equivalent days) were used to estimate cVMS SOA at

392   background and polar sites. Although there may be some uncertainties in extrapolating our results to the real

393   atmosphere, these extrapolations may still provide an estimation for understanding the SOA potential of

394   cVMS.

395   Table S6 summarizes the details regarding sites and concentrations of cVMS SOA. The derived

396   concentrations of cVMS SOA vary significantly among urban, background and polar sites. The total cVMS

397   SOA concentrations in urban areas are the highest, up to 33.52 ng/m^3, which was comparable with the

398   maximum cVMS SOA formation (21 ng/m^3) reported by Pennington et al. (2021) using the CMAQ model

399   for Los Angeles. They are 0.57-8.86 and 0.37-1.97 ng/m^3 for background and Arctic sites, respectively.

400   cVMS SOA concentrations in urban regions of Asia (sites 29-36) and Europe (sites 26-28) are generally

401   larger than that of North America (sites 20-25). In China, the total cVMS SOA concentrations in urban sites

402   range from 0.11 to 33.52 ng/m^3. The main precursors of cVMS SOA are different among Chinese cities. For

403   three cities along the southeast coast of China (Guangzhou, Macau and Foshan), the dominant precursors of

404   cVMS SOA are D3 and D4, which are related to industrial emissions of these two siloxanes in this region

405   (Wang et al., 2001). For Dalian in China, D5 mainly contributes to cVMS SOA, and this can be attributed to

406   the industrial production and the use of personal care products in Dalian (Li et al., 2020). In the other Chinese

407   urban areas with reported cVMS concentrations (Lhasa, Golmud, Kunming and Yantai), the total cVMS

408 SOA concentrations are considerably smaller than those in the urban areas above, with D5 acting as the main

409 precursor, which may be ascribed to the relatively low population densities in these cities (Wang et al., 2018).

410
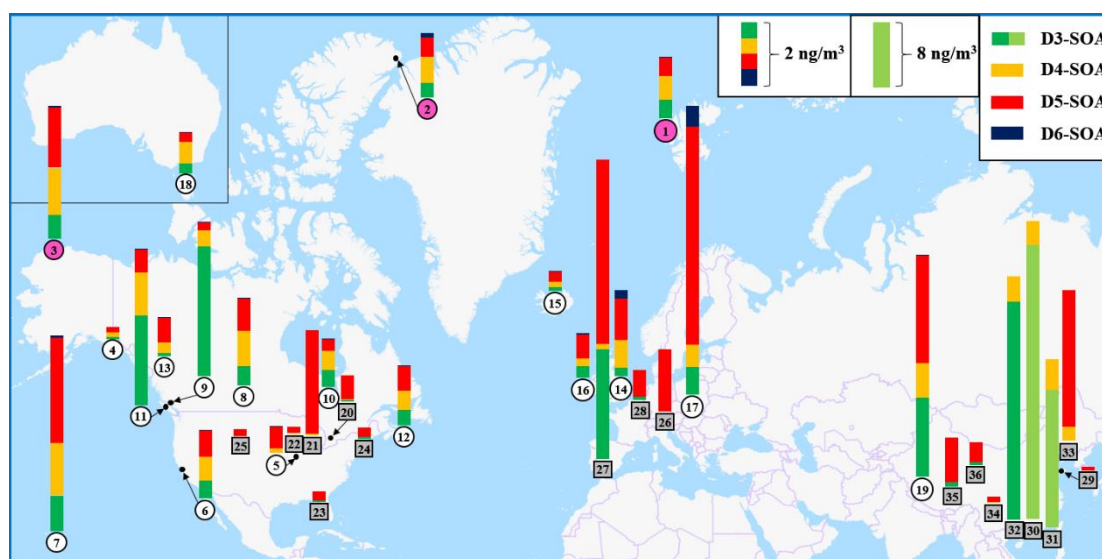
Figure 4. Global concentrations of cVMS SOA (ng/m³) on the basis of the cVMS concentrations

reported from multiple studies and the cVMS SOA yields measured in this work. The numbers of polar,

background and urban sites are enclosed in pink, white circles and gray boxes, respectively. The details

about cVMS and SOA concentrations at different sites were summarized in Table S6 of the Supplement.

415

416 At urban sites in Europe and North America, cVMS SOA concentrations are reported in the range of 0.91-

417 9.16 ng/m³ and 0.19-3.23 ng/m³, respectively. Among these cVMS, D5 is the main contributor to cVMS

418 SOA at these locations, averaging 89.1% of total cVMS SOA. For instance, D5 SOA is calculated to be 5.63

419 ng/m³ in Catalan, Spain, 3.19 ng/m³ in Chicago, USA, 1.89 ng/m³ in Zurich, Switzerland and 0.81 ng/m³ in

420 Paris, France, where there are high levels of economic activities and high population densities. These results

421 suggest that personal care products as a main source of D5 may be the most important anthropogenic origins

422 of Si-containing SOA in Europe and North America. The D5 SOA concentration (0.11-5.63 ng/m³) estimated

423 here is larger than that (0.016-0.206 ng/m³) reported by Milani et al. (2021), who obtained their data using

424   semi-quantified concentrations of D_4TOH (first-generation D5 SOA product) extracted from $PM_{2.5}$ samples

425   in Atlanta and Houston. The difference may be mainly attributed to the missing analysis of multi-generation

426   SOA products or dimers (Wu and Johnston, 2016, 2017).

427   At background and Arctic sites, cVMS SOA are primarily derived from D3, D4 and D5. The background

428   sites are located in mountains, rural areas, forested areas, lakes and at high altitudes. The three highest cVMS

429   SOA concentrations at background sites are located at Kosetice in the Czech Republic (8.86 ng/m^3), Tibetan

430   Plateau in China (6.78 ng/m^3) and Hilo of Hawaii in the USA (5.97 ng/m^3), where the contribution

431   percentages of SOA from D3-D5 are 92.8%, 99.9% and 99.0%, respectively. The cVMS SOA concentrations

432   at the Alert site in Nunavut, Canada is the highest (1.97 ng/m^3) among the three locations in the Arctic, 92.4%

433   of which is accounted for by D3-D5 SOA. The dominance of D3-D5 SOA in both background and the Arctic

434   regions highlights their persistence in the atmosphere and the potential for long-range atmospheric transport.

435   The global annual production of D4, D5 and D6 is about 1, 0.1 and 0.01 Tg·yr^{-1}, respectively, and 90% of

436   these cVMS is eventually released into the atmosphere (Li et al., 2020; Genualdi et al., 2011; Wang et al.,

437   2013; Sakurai et al., 2019). Based on the results shown in Fig. 4, the annual production of cVMS (D4-D6)

438   SOA was estimated to be 0.01 Tg·yr^{-1}, which was about 0.34% of SOA (2.9 Tg·yr^{-1}) produced from mobile

439   source emissions in the USA and 33%-50% of SOA generated by Athabasca oil sands (0.02-0.03 Tg·yr^{-1},

440   one of the largest sources of anthropogenic secondary organic aerosols in North America) (Tkacik et al.,

441   2014; Liggio et al., 2016). Moreover, it was 0.05% and 0.14% of isoprene-SOA (20 Tg·yr^{-1}) and

442   monoterpenes-SOA (7 Tg·yr^{-1}) (typical biogenic SOA), respectively, indicating the potential importance of

443   cVMS SOA (Jokinen et al., 2015). While these cVMS SOA sources may seem small, they can make

444   substantially higher contributions to ambient air SOAs in population centers where cVMS compounds are

445   primarily used.

446

Author contributions

CH designed and conducted all experiments; CH and HY analyzed the data and prepared the paper with

contributions from KL, PL, JL, AL and SML. SML supervised the project.

450

Competing interests

The authors declare that they have no conflict of interest.

453

458

References

Ahrens, L., Harner, T., and Shoeib, M.: Temporal Variations of Cyclic and Linear Volatile Methylsiloxanes in the Atmosphere Using Passive Samplers and High-Volume Air Samplers, Environ. Sci. Technol., 48, 9374-9381, https://doi.org/10.1021/es502081j, 2014.

Allen, R., Kochs, P., and Chandra, G.: Industrial Organosilicon Materials, Their Environmental Entry and Predicted Fate, Springer, 3, 1-25, https://doi.org/10.1007/978-3-540-68331-5_1, 1997.

Alton, M. and Browne, E.: Atmospheric Chemistry of Volatile Methyl Siloxanes: Kinetics and Products of Oxidation by OH Radicals and Cl Atoms, Environ. Sci. Technol., 54, 5992-5999, https://dx.doi.org/10.1021/acs.est.0c01368, 2020.

Atkinson, R.: Kinetics of the Gas-Phase Reactions of a Series of Organosilicon Compounds with OH and NO_3 Radicals and O_3 at 297 ± 2 K, Environ. Sci. Technol., 25, 863-866, https://doi.org/10.1021/es00017a005, 1991.

Bein, K., Zhao, Y., Wexler, A., Johnston, M.: Speciation of Size-Resolved Individual Ultrafine Particles in

Pittsburgh, Pennsylvania, J. Geophys. Res., 110, D07S05, https://doi.org/10.1029/2004jd004708, 2005.

Berndt, T., Richters, S., Jokinen, T., Hyttinen, N., Kurtén, T., Otkjaer, R., Kjaergaard, H., Stratmann, F., Herrmann, H., Sipilä, M., Kulmala, M., and Ehn, M.: Hydroxyl Radical-Induced Formation of Highly Oxidized Organic Compounds, Nat. Commun., 7, 1-8, https://doi.org/10.1038/ncomms13677, 2016.

Bruns, E., Haddad, I., Keller, A., Klein, F., Kumar, N., Pieber, S., Corbin, J., Slowik, J., Brune, W., Baltensperger, U., and Prévôt, A.: Inter-Comparison of Laboratory Smog Chamber and Flow Reactor Systems on Organic Aerosol Yield and Composition, Atmos. Meas. Tech., 8, 2315-2332, https://doi.org/10.5194/amt-8-2315-2015, 2015.

Bzdek, B., Horan, A., Pennington, M., Janechek, N., Baek, J., Stanier, C., and Johnston, M.: Silicon is a Frequent Component of Atmospheric Nanoparticles, Environ. Sci. Technol., 48, 11137-11145, https://doi.org/10.1021/es5026933, 2014.

Canada, E. C. a. H.: https://www.ec.gc.ca/ese-ees/FC0D11E7-DB34-41AA-B1B3-E66EFD8813F1/batch2_540-97-6_en.pdf last access: 9 February 2022, 2008.

Chan, A., Kautzman, K., Chhabra, P., Surratt, J., Chan, M., Crounse, J., Kürten, A., Wennberg, P., Flagan, R., and Seinfeld, J.: Secondary Organic Aerosol Formation from Photooxidation of Naphthalene and Alkylnaphthalenes: Implications for Oxidation of Intermediate Volatility Organic Compounds (IVOCs), Atmos. Chem. Phys., 9, 3049–3060, https://doi.org/10.5194/acp-9-3049-2009, 2009.

Chandramouli, B., Kamens, R.: The Photochemical Formation and Gas-Particle Partitioning of Oxidation Products of Decamethyl Cyclopentasiloxane and Decamethyl Tetrasiloxane in the Atmosphere, Atmos. Environ., 35, 87-95, https://doi.org/10.1016/S1352-2310(00)00289-2, 2001.

Charan, S., Huang, Y., Buenconsejo, R., Li, Q., Cocker Iii, D., and Seinfeld, J.: Secondary Organic Aerosol Formation from the Oxidation of Decamethylcyclopentasiloxane at Atmospherically Relevant OH Concentrations, Atmos. Chem. Phys., 22, 917-928, https://doi.org/10.5194/acp-22-917-2022, 2022.

Coggon, M., McDonald, B., Vlasenko, A., Veres, P., Bernard, F., Koss, A., Yuan, B., Gilman, J., Peischl, J., Aikin, K., DuRant, J., Warneke, C., Li, S.-M., and Gouw, J.: Diurnal Variability and Emission Pattern of Decamethylcyclopentasiloxane (D5) from the Application of Personal Care Products in Two North American Cities, Environ. Sci. Technol., 52, 5610-5618, https://doi.org/10.1021/acs.est.8b00506, 2018.

EUR-Lex: https://eur-lex.europa.eu/legal-content/EN/TXT/?uri=uriserv:OJ.L_.2018.006.01.0045.01.ENG&toc=OJ:L:2018:006:TOCECHA, last access: 25 November 2021, 2018.

501 Farasani, A. and Darbre, P.: Exposure to Cyclic Volatile Methylsiloxanes (cVMS) Causes Anchorage-Independent

502 Growth and Reduction of BRCA1 in Non-Transformed Human Breast Epithelial Cells, J. Appl. Toxicol., 37,

503 454-461, https://doi.org/10.1002/jat.3378, 2017.

504 Genualdi, S., Harner, T., Cheng, Y., Macleod, M., Hansen, K., Egmond, R., Shoeib, M., and Lee, S.: Global

505 Distribution of Linear and Cyclic Volatile Methyl Siloxanes in Air, Environ. Sci. Technol., 45, 3349-3354,

506 https://doi.org/10.1021/es200301j, 2011.

507 Glasius, M. and Goldstein, A.: Recent Discoveries and Future Challenges in Atmospheric Organic Chemistry,

508 Environ. Sci. Technol., 50, 2754-2764, https://doi.org/10.1021/acs.est.5b05105, 2016.

509 Guo, J., Zhou, Y., Cui, J., Zhang, B., and Zhang, J.: Assessment of Volatile Methylsiloxanes in Environmental

510 Matrices and Human Plasma, Sci. Total. Environ., 668, 1175-1182,

511 https://doi.org/10.1016/j.scitotenv.2019.03.092, 2019.

512 Huang, Y., Coggon, M., Zhao, R., Lignell, H., Bauer, M., Flagan, R., and Seinfeld, J.: The Caltech Photooxidation

513 Flow Tube reactor: Design, Fluid Dynamics and Characterization, Atmos. Meas. Tech., 10, 839-867,

514 https://doi.org/10.5194/amt-10-839-2017, 2017.

515 Janechek, N., Hansen, K., and Stanier, C.: Comprehensive Atmospheric Modeling of Reactive Cyclic Siloxanes

516 and their Oxidation Products, Atmos. Chem. Phys., 17, 8357-8370, https://doi.org/10.5194/acp-17-8357-2017,

517 2017.

518 Janechek, N., Marek, R., Bryngelson, N., Singh, A., Bullard, R., Brune, W., and Stanier, C.: Physical Properties

519 of Secondary Photochemical Aerosol from OH Oxidation of a Cyclic Siloxane, Atmos. Chem. Phys., 19, 1649-

520 1664, https://doi.org/10.5194/acp-19-1649-2019, 2019.

521 Jokinen, T., Berndt, T., Makkonen, R., Kerminen, V., Junninen, H., Paasonen, P., Stratmann, F., Herrmann, H.,

522 Guenther, A., Worsnop, D., Kulmala, M., Ehn, M., and Sipilä, M.: Production of Extremely Low Volatile

523 Organic Compounds from Biogenic Emissions: Measured Yields and Atmospheric Implications, Proc. Natl.

524 Acad. Sci. U S A., 112, 7123-7128, https://doi.org/10.1073/pnas.1423977112, 2015.

525 Kierkegaard, A. and McLachlan, M.: Determination of Linear and Cyclic Volatile Methylsiloxanes in Air at a

526 Regional Background Site in Sweden, Atmos. Environ., 80, 322-329,

527 https://doi.org/10.1016/j.atmosenv.2013.08.001, 2013.

528 Kim, J. and Xu, S.: Quantitative Structure-Reactivity Relationships of Hydroxyl Radical Rate Constants for Linear

529 and Cyclic Volatile Methylsiloxanes, Environ. Toxicol. Chem., 36, 3240-3245, https://doi.org/10.1002/etc.3914,

530 2017.

531 Kim, J., Mackay, D., and Whelan, M.: Predicted Persistence and Response Times of Linear and Cyclic Volatile

532 Methylsiloxanes in Global and Local Environments, Chemosphere, 195, 325-335,

533 https://doi.org/10.1016/j.chemosphere.2017.12.071, 2018.

534 Krogseth, I., Zhang, X., Lei, Y., Wania, F., and Breivik, K.: Calibration and Application of a Passive Air Sampler

535 (XAD-PAS) for Volatile Methyl Siloxanes, Environ. Sci. Technol., 47, 4463-4470,

536 https://doi.org/10.1021/es400427h, 2013a.

537 Krogseth, I., Kierkegaard, A., McLachlan, M., Breivik, K., Hansen, K., and Schlabach, M.: Occurrence and

538 Seasonality of Cyclic Volatile Methyl Siloxanes in Arctic Air, Environ. Sci. Technol., 47, 502-509,

539 https://doi.org/10.1021/es3040208, 2013b.

540 Lambe, A., Chhabra, P., Onasch, T., Brune, W., Hunter, J., Kroll, J., Cummings, M., Brogan, J., Parmar, Y.,

541 Worsnop, D., Kolb, C., and Davidovits, P.: Effect of Oxidant Concentration, Exposure Time, and Seed Particles

542 on Secondary Organic Aerosol Chemical Composition and Yield, Atmos. Chem. Phys., 15, 3063-3075,

543 https://doi.org/10.5194/acp-15-3063-2015, 2015.

544 Lambe, A., Ahern, A., Williams, L., Slowik, J., Wong, J., Abbatt, J., Brune, W., Ng, N., Wright, J., Croasdale, D.,

545 Worsnop, D., Davidovits, P., and Onasch, T.: Characterization of Aerosol Photooxidation Flow Reactors:

546 Heterogeneous Oxidation, Secondary Organic Aerosol Formation and Cloud Condensation Nuclei Activity

547 Measurements, Atmos. Meas. Tech., 4, 445-461, https://doi.org/10.5194/amt-4-445-2011, 2011.

548 Lambe, A., Massoli, P., Zhang, X., Canagaratna, M., Nowak, J., Daube, C., Yan, C., Nie, W., Onasch, T., Jayne,

549 J., Kolb, C., Davidovits, P., Worsnop, D., and Brune, W.: Controlled Nitric Oxide Production via $O(^1D) + N_2O$

550 Reactions for Use in Oxidation Flow Reactor Studies, Atmos. Meas. Tech., 10, 2283-2298,

551 https://doi.org/10.5194/amt-10-2283-2017, 2017.

552 Lamkaddam, H., Gratien, A., Pangui, E., Cazaunau, M., Varrault, B., and Doussin, J.: High-NO_x Photooxidation

553 of n-Dodecane: Temperature Dependence of SOA Formation, Environ Sci Technol, 51, 192-201,

554 https://doi.org/10.1021/acs.est.6b03821, 2017.

555 Lee, A., Hayden, K., Herckes, P., Leaitch, W., Liggio, J., Macdonald, A., and Abbatt, J.: Characterization of

556 Aerosol and Cloud Water at a Mountain Site During WACS 2010: Secondary Organic Aerosol Formation

557 through Oxidative Cloud Processing, Atmos. Chem. Phys., 12, 7103-7116, https://doi.org/10.5194/acp-12-

558 7103-2012, 2012.

559 Li, K., Liggio, J., Lee, P., Han, C., Liu, Q., and Li, S.-M.: Secondary Organic Aerosol Formation from α-Pinene,

560 Alkanes, and Oil Sand-Related Precursors in a New Oxidation Flow Reactor, Atmos. Chem. Phys., 19, 9715-

561 9731, https://doi.org/10.5194/acp-19-9715-2019, 2019a.

562 Li, K., Liggio, J., Han, C., Liu, Q., Moussa, S., Lee, P., and Li, S.-M.: Understanding the Impact of High-NO$_x$

563 Conditions on the Formation of Secondary Organic Aerosol in the Photooxidation of Oil Sand-Related

564 Precursors, Environ. Sci. Technol., 53, 14420-14429, https://doi.org/10.1021/acs.est.9b05404, 2019b.

565 Li, Q., Lan, Y., Liu, Z., Wang, X., Wang, X., Hu, J., and Geng, H.: Cyclic Volatile Methylsiloxanes (cVMSs) in

566 the Air of the Wastewater Treatment Plants in Dalian, China-Levels, Emissions, and Trends, Chemosphere, 256,

567 1-8, https://doi.org/10.1016/j.chemosphere.2020.127064, 2020.

568 Li, S.-M. and Winchester, J.: Particle Size Distribution and Chemistry of Late Winter Arctic Aerosols, J. Geophys.

569 Res., 95, 13897-13908, https://doi.org/10.1029/J095iD09p13897, 1990.

570 Li, S.-M. and Winchester, J.: Aerosol Silicon and Associated Elements in the Arctic High and Mid-Troposphere,

571 Atmos. Environ., 27, 2907-2912, https://doi.org/10.1016/0960-1686(93)90322-P, 1993.

572 Liggio, J., Li, S.-M., Hayden, K., Taha, Y., Stroud, C., Darlington, A., Drollette, B., Gordon, M., Lee, P., Liu, P.,

573 Leithead, A., Moussa, S., Wang, D., Brien, J., Mittermeier, R., Brook, J., Lu, G., Staebler, R., Han, Y., Tokarek,

574 T., Osthoff, H., Makar, P., Zhang, J., Plata, D., and Gentner, D.: Oil Sands Operations as a Large Source of

575 Secondary Organic Aerosols, Nature, 534, 91-94, https://doi.org/10.1038/nature17646, 2016.

576 Liu, N., Xu, L., and Cai, Y.: Methyl Siloxanes in Barbershops and Residence Indoor Dust and the Implication for

577 Human Exposures, Sci. Total. Environ., 618, 1324-1330, https://doi.org/10.1016/j.scitotenv.2017.09.250, 2018.

578 Mao, J., Ren, X., Brune, W., Olson, J., Crawford, J., Fried, A., Huey, L., Cohen, R., Heikes, B., Singh, H., Blake,

579 D., Sachse, G., Diskin, G., Hall, S., and Shetter, R.: Airborne Measurement of OH Reactivity during INTEX-

580 B, Atmos. Chem. Phys., 9, 163-173, https://doi.org/10.5194/acp-9-163-2009, 2009.

581 McFiggans, G., Mentel, T., Wildt, J., Pullinen, I., Kang, S., Kleist, E., Schmitt, S., Springer, M., Tillmann, R., Wu,

582 C., Zhao, D., Hallquist, M., Faxon, C., Breton, M., Hallquist, A., Simpson, D., Bergström, R., Jenkin, M., Ehn,

583 M., Thornton, J., Alfarra, M., Bannan, T., Percival, C., Priestley, M., Topping, D., and Scharr, A.: Secondary

584 Organic Aerosol Reduced by Mixture of Atmospheric Vapours, Nature, 565, 587-593,

585 https://doi.org/10.1038/s41586-018-0871-y, 2019.

586 Milani, A., Al-Naiema, I., and Stone, E.: Detection of a Secondary Organic Aerosol Tracer Derived from Personal

587 Care Products, Atmos. Environ., 246, https://doi.org/10.1016/j.atmosenv.2020.118078, 2021.

588 Ng, N., Kroll, J., Chan, A., Chhabra, P., Flagan, R., and Seinfeld, J.: Secondary Organic Aerosol Formation from

589 m-Xylene, Toluene, and Benzene, Atmos. Chem. Phys., 7, 3909–3922, https://doi.org/10.5194/acp-7-3909-

590 2007, 2007a.

591   Ng, N., Chhabra, P., Chan, A., Surratt, J., Kroll, J., Kwan, A., McCabe, D., Wennberg, P., Sorooshian, A., Murphy,

592   S., Dalleska, N., Flagan, R., and Seinfeld, J.: Effect of NO_x Level on Secondary Organic Aerosol (SOA)

593   Formation from the Photooxidation of Terpenes, Atmos. Chem. Phys., 7, 5159–5174,

594   https://doi.org/10.5194/acp-7-5159-2007, 2007b.

595   Ng, N., Canagaratna, M., Zhang, Q., Jimenez, J., Tian, J., Ulbrich, I., Kroll, J., Docherty, K., Chhabra, P., Bahreini,

596   R., Murphy, S., Seinfeld, J., Hildebrandt, L., Donahue, N., DeCarlo, P., Lanz, V., Prévôt, A., Dinar, E., Rudich,

597   Y., and Worsnop, D.: Organic Aerosol Components Observed in Northern Hemispheric Datasets from Aerosol

598   Mass Spectrometry, Atmos. Chem. Phys., 10, 4625-4641, https://doi.org/10.5194/acp-10-4625-2010, 2010.

599   Peng, Z., Taylor, J., Orlando, J., Tyndall, G., and Jimenez, J.: Organic Peroxy Radical Chemistry in Oxidation

600   Flow Reactors and Environmental Chambers and their Atmospheric Relevance, Atmos. Chem. Phys., 19, 813-

601   834, https://doi.org/10.5194/acp-19-813-2019, 2019.

602   Peng, Z., Palm, B., Day, D., Talukdar, R., Hu, W., Lambe, A., Brune, W., and Jimenez, J.: Model Evaluation of

603   New Techniques for Maintaining High-NO Conditions in Oxidation Flow Reactors for the Study of OH-

604   Initiated Atmospheric Chemistry, ACS. Earth. Space. Chem. , 2, 72-86,

605   https://doi.org/10.1021/acsearthspacechem.7b00070, 2018.

606   Pennington, E., Seltzer, K., Murphy, B., Qin, M., Seinfeld, J., and Pye, H.: Modeling Secondary Organic Aerosol

607   Formation from Volatile Chemical Products, Atmos. Chem. Phys., 21, 18247-18261,

608   https://doi.org/10.5194/acp-21-18247-2021, 2021.

609   Phares, D., Rhoads, K., Johnston, M., and Wexler, A.: Size-Resolved Ultrafine Particle Composition Analysis 2.

610   Houston, J. Geophys. Res., 108, 1-14, https://doi.org/10.1029/2001jd001212, 2003.

611   Presto, A., Hartz, K., and Donahue, N.: Secondary Organic Aerosol Production from Terpene Ozonolysis. 2. Effect

612   of NO_x Concentration, Environ. Sci. Technol. , 39, 7046-7054, https://doi.org/10.1021/es050400s, 2005.

613   Rauert, C., Shoieb, M., Schuster, J., Eng, A., and Harner, T.: Atmospheric Concentrations and Trends of Poly- and

614   Perfluoroalkyl Substances (PFAS) and Volatile Methyl Siloxanes (VMS) over 7 Years of Sampling in the Global

615   Atmospheric Passive Sampling (GAPS) Network, Environ. Pollut., 238, 94-102,

616   https://doi.org/10.1016/j.envpol.2018.03.017, 2018.

617   Rhoads, K., Phares, D., Wexler, A., Johnston, M.: Size-Resolved Ultrafine Particle Composition Analysis 1.

618   Atlanta, J. Geophys. Res., 108, 1-13, https://doi.org/10.1029/2001jd001211, 2003.

619   Riipinen, I., Juuti, T., Pierce, J., Petäjä, T., Worsnop, D., Kulmala, M., and Donahue, N.: The Contribution of

620   Organics to Atmospheric Nanoparticle Growth, Nat. Geosci., 5, 453-458, https://doi.org/10.1038/ngeo1499,

621   2012.

622   Rücker, C. and Kümmerer, K.: Environmental Chemistry of Organosiloxanes, Chem. Rev., 115, 466-524,

623   https://doi.org/10.1021/cr500319v, 2015.

624   Safron, A., Strandell, M., Kierkegaard, A., and Macleod, M.: Rate Constants and Activation Energies for Gas-

625   Phase Reactions of Three Cyclic Volatile Methyl Siloxanes with the Hydroxyl Radical, Int. J. Chem. Kinet., 47,

626   420-428, https://doi.org/10.1002/kin.20919, 2015.

627   Sakurai, T., Imaizumi, Y., Kuroda, K., Hayashi, T., and Suzuki, N.: Georeferenced multimedia environmental fate

628   of volatile methylsiloxanes modeled in the populous Tokyo Bay catchment basin, Sci Total Environ, 689, 843-

629   853, https://doi.org/10.1016/j.scitotenv.2019.06.462, 2019.

630   Sarrafzadeh, M., Wildt, J., Pullinen, I., Springer, M., Kleist, E., Tillmann, R., Schmitt, S., Wu, C., Mentel, T., Zhao,

631   D., Hastie, D., and Scharr, A.: Impact of NO_x and OH on Secondary Organic Aerosol Formation from β-Pinene

632   Photooxidation, Atmos. Chem. Phys., 16, 11237-11248, https://doi.org/10.5194/acp-16-11237-2016, 2016.

633   Simonen, P., Saukko, E., Karjalainen, P., Timonen, H., Bloss, M., Saksa, P., Rönkkö, T., Keskinen, J., and Maso,

634   M.: A New Oxidation Flow Reactor for Measuring Secondary Aerosol Formation of Rapidly Changing

635   Emission Sources, Atmos. Meas. Tech., 10, 1519-1537, https://doi.org/10.5194/amt-10-1519-2017, 2017.

636   Sommerlade, R., Parlar, H., Wrobel, D , Kochs, P.: Product Analysis and Kinetics of the Gas-Phase Reactions of

637   Selected Organosilicon Compounds with OH Radicals Using a Smog Chamber-Mass Spectrometer System,

638   Environ. Sci. Technol., 27, 2435-2440, https://doi.org/10.1021/es00048a019, 1993.

639   Tang, X., Misztal, P., Nazaroff, W., and Goldstein, A.: Siloxanes Are the Most Abundant Volatile Organic

640   Compound Emitted from Engineering Students in a Classroom, Environ. Sci. Technol. Lett. , 2, 303-307,

641   https://doi.org/10.1021/acs.estlett.5b00256, 2015.

642   Tkacik, D., Lambe, A., Jathar, S., Li, X., Presto, A., Zhao, Y., Blake, D., Meinardi, S., Jayne, J., Croteau, P., and

643   Robinson, A.: Secondary Organic Aerosol Formation from in-Use Motor Vehicle Emissions Using a Potential

644   Aerosol Mass Reactor, Environ. Sci. Technol., 48, 11235-11242, https://doi.org/10.1021/es502239v, 2014.

645   Wang, D.-G., Norwood, W., Alaee, M., Byer, J., and Brimble, S.: Review of Recent Advances in Research on the

646   Toxicity, Detection, Occurrence and Fate of Cyclic Volatile Methyl Siloxanes in the Environment, Chemosphere,

647   93, 711-725, https://doi.org/10.1016/j.chemosphere.2012.10.041, 2013.

648   Wang, X., Schuster, J., Jones, K., and Gong, P.: Occurrence and Spatial Distribution of Neutral Perfluoroalkyl

649   Substances and Cyclic Volatile Methylsiloxanes in the Atmosphere of the Tibetan Plateau, Atmos. Chem. Phys.,

650   18, 8745-8755, https://doi.org/10.5194/acp-18-8745-2018, 2018.

651 Wang, X., Lee, S., Sheng, G., Chan, L., Fu, J., Li, X., Min, Y., and Chan, C.: Cyclic organosilicon compounds in

652 ambient air in Guangzhou, Macau and Nanhai, Pearl River Delta, Appl. Geochemistry, 16, 1447-1454,

653 https://doi.org/10.1016/S0883-2927(01)00044-0, 2001.

654 Wildt, J., Mentel, T., Scharr, A., Hoffmann, T., Andres, S., Ehn, M., Kleist, E., Müsgen, P., Rohrer, F., Rudich, Y.,

655 Springer, M., Tillmann, R., and Wahner, A.: Suppression of New Particle Formation from Monoterpene

656 Oxidation by NO_x, Atmos. Chem. Phys., 14, 2789-2804, https://doi.org/10.5194/acp-14-2789-2014, 2014.

657 Wu, Y. and Johnston, M.: Molecular Characterization of Secondary Aerosol from Oxidation of Cyclic

658 Methylsiloxanes, J. Am. Soc. Mass Spectrom., 27, 402-409, https://doi.org/10.1007/s13361-015-1300-1, 2016.

659 Wu, Y. and Johnston, M.: Aerosol Formation from OH Oxidation of the Volatile Cyclic Methyl Siloxane (cVMS)

660 Decamethylcyclopentasiloxane, Environ. Sci. Technol., 51, 4445-4451,

661 https://doi.org/10.1021/acs.est.7b00655, 2017.

662 Xiao, R., Zammit, I., Wei, Z., Hu, W.-P., MacLeod, M., and Spinney, R.: Kinetics and Mechanism of the Oxidation

663 of Cyclic Methylsiloxanes by Hydroxyl Radical in the Gas Phase: An Experimental and Theoretical Study,

664 Environ. Sci. Technol., 49, 13322-13330, https://doi.org/10.1021/acs.est.5b03744, 2015.

665 Xu, S., Warner, N., Nizzetto, P., Durham, J., and McNett, D.: Long-Range Transport Potential and Atmospheric

666 Persistence of Cyclic Volatile Methylsiloxanes Based on Global Measurements, Chemosphere, 228, 460-468,

667 https://doi.org/10.1016/j.chemosphere.2019.04.130, 2019.

668 Zhao, D., Schmitt, S., Wang, M., Acir, I., Tillmann, R., Tan, Z., Novelli, A., Fuchs, H., Pullinen, I., Wegener, R.,

669 Rohrer, F., Wildt, J., Scharr, A., Wahner, A., and Mentel, T.: Effects of NO_x and SO_2 on the Secondary Organic

670 Aerosol Formation from Photooxidation of α-Pinene and Limonene, Atmos. Chem. Phys., 18, 1611-1628,

671 https://doi.org/10.5194/acp-18-1611-2018, 2018.

672 Zhou, C., Jang, M., and Yu, Z.: Simulation of SOA Formation from the Photooxidation of Monoalkylbenzenes in

673 the Presence of Aqueous Aerosols Containing Electrolytes under Various NO_x Levels, Atmos. Chem. Phys., 19,

674 5719-5735, https://doi.org/10.5194/acp-19-5719-2019, 2019.